Analytical derivation of the impulse response for the bounded 2-D diffusion channel

Fatih Dinc, Bayram Cevdet Akdeniz, Ecda Erol, Dilara Gokay, Ezgi Tekgul, Ali Emre Pusane, Tuna Tugcu

Analytical Derivation of the Impulse Response for the Bounded 2-D Diffusion Channel

Fatih Dinc[1,2], Bayram Cevdet Akdeniz[1], Ecda Erol[3], Dilara Gokay[4], Ezgi Tekgul[1], Ali Emre Pusane[1], and Tuna Tugcu[5]

[1]Department of Electrical & Electronics Engineering, Bogazici University, Istanbul, 34342, Turkey
[2]Perimeter Institute for Theoretical Physics, Waterloo, Ontario, N2L 2Y5, Canada
[3]Department of Mechanical Engineering, Bogazici University, Istanbul, 34342, Turkey
[4]Department of Computer Engineering, Bogazici University, Istanbul, 34342, Turkey
[5]Department of Computer Engineering, NETLAB, Bogazici University, Istanbul, 34342, Turkey

Version: February 17, 2019

Abstract

This letter focuses on the derivation of the hitting probabilities of diffusing particles absorbed by an agent in a bounded environment. In particular, we analogously consider the impulse response of a molecular communication channel in a 2-D and 3-D environment. In 2-D, the channel involves a point transmitter that releases molecules to a circular absorbing receiver that absorbs incoming molecules in an environment surrounded by a circular reflecting boundary. Considering this setup, the joint distribution of the molecules on the circular absorbing receiver with respect to time and angle is derived. Using this distribution, the channel characteristics are examined. Then, we extend this channel model to 3-D using a cylindrical receiver and investigate the channel properties. We also propose how to obtain an ~~near-exact~~ analytic estimate for the unbounded 2-D channel from our derived solutions, as no analytic derivation for this channel is present in the literature. Throughout the letter, we perform particle-based simulations to compare the analytic results and lay evidence for our findings.

1 Introduction

Molecular communication (MC) has recently gained much attention as a promising method for communication among nanodevices. A method of such communication is the diffusion of molecules in biological environments, where the messenger molecules are used to mediate signals between transmitters and receivers. Medical applications constitute a promising application field for such biocompatible nanodevices. Therefore, examining the response of molecular communication channels is an important task to determine communication characteristics and possible communication scenarios. Fortunately, Brownian motion has been explored extensively in the physics literature in the context of first passage processes [1, 2, 3, 4, 5]. As they describe the hitting probability in diffusive environments, the first-passage processes found many applications in the molecular communication literature to describe diffusion channels consisting of transmitters and receivers [6, 7, 8].

Many different types of receivers have been extensively explored in the molecular communication literature [9, 10, 11, 12]. Among those, two are more commonly utilized: absorbing receivers that consume the incoming molecules upon contact and observing receivers that track the number of molecules inside a volume without absorbing them. In the literature, impulse responses for both types of channel models have been investigated in great detail. In general, these channels can be categorized into two groups according to their environments as well. While some channels are placed in a free unbounded environment, others are placed in a bounded (and usually tubular) environment. For the first group, the impulse response for a 1-D channel is derived [13], while in [14] the 3-D channel's impulse response is examined for a point transmitter and a spherical absorbing receiver. Nevertheless, the impulse response in a 2-D unbounded medium for a point transmitter and a circular absorbing receiver has not been derived, except for some special cases presented in [15, 16]. The channels with point transmitters, as well as the ones with spherical transmitters, are considered in a 3-D medium in [17] and [18].

As stated in [19], vessel-like channels, one type of bounded channels, have beneficial effects for long-range molecular communication by preserving released molecules in a bounded range. Therefore, they have higher

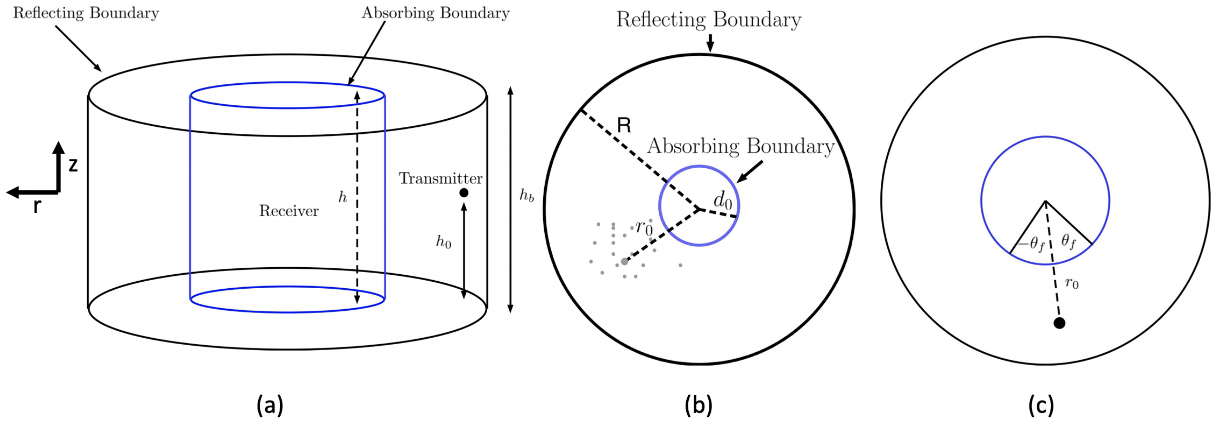

Figure 1: (a) General Channel Model for a point transmitter situated at $r = r_0$, a cylindrical absorbing receiver with radius d_0 and height h surrounded by a larger cylindrical reflecting walls with radius R and height h. Note that the diffusion of the molecules is confined inside a finite annular volume depicted in (b) as the z-dependence is suppressed through symmetry arguments. (c) The receiver can be modified to count only the particles inside the angle range $(-\theta_f, \theta_f)$.

power efficiency, which is one of the reasons why many biological systems evolved in this direction. Since the molecules are not dispersed too much compared to the case of unbounded environments and due to their possible practical use in health applications, bounded and particularly vessel-like channels gained much attention in the literature. In [20], the 1-D and 3-D hitting location distributions of messenger molecules on a planar receiver are examined when there is no flow in the vessel-like environment. In [21], the impulse response of a 3-D vessel-like channel is obtained for a spherical observing receiver when there is a laminar flow in the environment. In [22], the flow models for microfluidic channels with different cross-sectional areas are presented, and the impulse response is derived by solving the 1-D diffusion-advection equation, which is only valid for some specific cases. Besides the channel impulse response, the capacity of the single-input single-output molecular communication channels with flow and drift is derived in [23].

In addition to vessel-like channels, diffusion processes that are bounded by membranes are also encountered commonly in nature. One such example is the transmission of messengers inside a spherical cell bounded by the cell membrane to an organelle, which can be modeled by a diffusion channel consisting of an absorbing spherical receiver and a reflecting/absorbing spherical boundary [24, 25]. In general, the spherical model is not always accurate to describe the diffusion processes inside the cell. In some cases, a cylindrical cell model can be more accurate, as there are many cylindrical structures in living organisms, like oval cells in the liver or simple columnar epithelium. Hence, the impulse response of a bounded cylindrical environment can be useful to describe diffusion processes inside such environments more accurately.

In this letter, we first derive the SO(2) symmetric[1] impulse response of a 2-D annular channel that consists of an absorbing circular receiver, a reflecting circular boundary and a point transmitter. Then, we find the channel characteristics of such a system and discuss many effects that arise due to the existence of the circular boundary. Afterwards, we derive the generalized angle-dependent impulse response for the annular channel, where the receiver only counts certain particles, which are absorbed inside the angle range $[-\theta_f, \theta_f]$. Next, we use the impulse response of the 2-D annular channel to find an analytic estimate with an arbitrarily small error for a circular receiver located in a 2-D unbounded channel, an exact analytic result which does not exist in the literature. As the impulse response of the 2-D bounded channel can be simulated via particle-based simulations, we perform further analysis to illustrate the accuracy of the analytic estimate. Later, we consider the 3-D concentric cylindrical diffusion channel that involves a point transmitter, a cylindrical absorbing receiver, and a cylindrical reflecting boundary. We show that the 3-D cylindrical channel can be described by the impulse response of the 2-D annular channel under certain assumptions. Finally, we conclude with further remarks on our findings and future work.

2 System Models

The system models for various channels considered in this letter are depicted in Fig.1. In this letter, we will simplify a 3-D coaxial cylindrical channel to a 2-D annular channel by certain assumptions and carry out the derivations for the impulse response of the 2-D channel. In the 3-D channel, shown in Fig. 1(a), a coaxial

[1] SO(2) symmetry in a 2-D coordinate system corresponds to the angular symmetry around the origin.

cylindrical absorbing receiver is placed at the center of the microfluidic channel whose boundary is reflecting and a point transmitter transmits messages by releasing molecules to the diffusion channel. Assuming that there is no flow in the environment, the propagation of the released molecules is modeled by Brownian Motion as

$$\Delta x \sim \mathcal{N}\left(0, 2D\Delta t\right), \tag{1a}$$
$$\Delta y \sim \mathcal{N}\left(0, 2D\Delta t\right), \tag{1b}$$
$$\Delta z \sim \mathcal{N}\left(0, 2D\Delta t\right), \tag{1c}$$

where D is diffusion coefficient, Δx, Δy and Δz are incremental step sizes in the three dimensions, Δt is time step, and $\mathcal{N}(\mu, \sigma^2)$ is the normal distribution with mean μ and variance σ^2. The cylindrical receiver absorbs the molecules that come to the vicinity of its receptors and makes a decision by counting these absorbed molecules. If the heights of the boundary h_b and the receiver h are equal, this system can be reduced to a 2-D bounded environment that has a concentric absorbing receiver and reflecting boundary as shown in Fig. 1(b). In practice, the length of the receiver can be smaller than the length of the channel as in the case of oval cells. Therefore, we shall evaluate the required condition for the height of the receiver h and height of the position of the transmitter h_0 for justifying the reduction this system to 2-D. The distribution of the released molecules along the z-axis can be modeled using (1) as $\mathcal{N}\left(h_0, 2Dt\right)$. Therefore, if the arrival probability of any molecule at either of the ends of the receiver is almost 0, then our approximation is still valid. Nonetheless, we stress that this is a simplifying assumption, as the diffusion along the z-axis is not independent of the absorption of molecules by the receiver. In fact, this assumption will lead to an over-estimate of the error bound, as we shall illustrate in Section 4.3. For now, we assume that we can reduce the microfluidic channel to 2-D with a coaxial cylindrical receiver if the following condition

$$P\left(z < 0\right) + P\left(z > h\right) < \epsilon \tag{2}$$

is satisfied. Then, using the distribution of z, we can write this condition explicitly as

$$Q\left(\frac{h_0}{\sqrt{2Dt}}\right) + Q\left(\frac{h - h_0}{\sqrt{2Dt}}\right) < \epsilon, \tag{3}$$

where t represents the maximum time of interest. Taking $h_0 = h/2$, one obtains

$$2Q\left(\frac{h}{2\sqrt{2Dt}}\right) < \epsilon. \tag{4}$$

Therefore, with the simplifying assumption $h \gg 2\sqrt{2Dt}$, the system can be reduced to 2-D. We shall first discuss the 2-D annular channel and then generalize its applications to various other channels: the 2-D annular channel with a partially absorbing receiver (with an angle-dependent impulse response), as an estimate for the impulse response of the 2-D unbounded channel with an absorbing receiver, and finally the 3-D channel with a coaxial cylindrical receiver.

3 2-D Annular Channel

3.1 Channel Impulse Response

In this section, we start by finding an impulse response for a 2-D annular channel, as depicted in Fig. 1(b), while deriving the probability density function of the molecules. To describe the diffusion of a molecule inside the annular region, we shall find a solution to Fick's Law

$$D\boldsymbol{\nabla}^2 P\left(r, t|r_0\right) = \frac{\partial P\left(r, t|r_0\right)}{\partial t}, \tag{5}$$

where $\boldsymbol{\nabla}^2$ is the Laplacian operator and $P\left(r, t|r_0\right)$ is the probability density function (PDF) of the molecules inside the diffusion channel. The circular boundary at $r = R$ is reflecting. Furthermore, the transmitter is assumed to be situated at a distance $r = r_0$ from the origin. In this section, we are interested in the absorption probability (an angle-independent quantity, see [14]) of the molecules by the receiver. Therefore, our calculations include an SO(2) symmetry. The physical meaning of this is the following: Instead of releasing molecules from a single point transmitter at a distance r_0 from the origin, we release them on a circle with radius r_0 according to a uniform angular distribution. Even though implementing this process could be physically more challenging, this assumption simplifies the theoretical problem significantly. As the receiver consumes molecules from all angles upon contact, both original and SO(2) symmetric problem will lead to the same absorption probability at a given time. In Section 4.1, the angle of absorption will be of interest as we discuss a partially absorbing receiver; hence, we will remove the SO(2) symmetry assumption there. In addition to the initial condition the probability distribution $P\left(r, t|r_0\right)$ should be zero when the molecules hit the receiver, where we assume a perfect receiver due to simplicity. This results in the boundary conditions

$$\frac{\partial P\left(r, t|r_0\right)}{\partial r}\bigg|_{r=R} = 0, \tag{6a}$$

$$P\left(r, t|r_0\right)\bigg|_{r=d_0} = 0, \tag{6b}$$

$$P(r, 0|r_0) = \frac{1}{2\pi r}\delta(r - r_0). \tag{6c}$$

We recall that, since the boundary is described by a mixture of Neumann and Dirichlet boundary conditions, the Laplacian operator is guaranteed to have a unique solution by the uniqueness theorem for the 3-D diffusion/heat equation [26].

Now, we shall start with the separation of variables Ansatz

$$P\left(r, t|r_0\right) = \phi(r, \theta)T(t), \tag{7}$$

which leads to the equation

$$D\frac{\boldsymbol{\nabla}^2\phi(r, \theta)}{\phi(r, \theta)} = \frac{T'(t)}{T(t)} = -\mu^2, \tag{8}$$

from which we can easily deduce

$$T(t) = Ae^{-\mu^2 t}, \tag{9}$$

where A and μ are constants. Afterwards, we arrive at the eigenvalue problem for the Laplacian operator

$$\boldsymbol{\nabla}^2\phi(r, \theta) = -\frac{\mu^2}{D}\phi(r, \theta). \tag{10}$$

We note that the overall factor of the solution is lumped into the time portion, $T(t)$. Therefore, we can arbitrarily normalize the space part, $\phi(r, t)$.

The eigenvalues μ^2/D are non-negative and real as either Neumann or Dirichlet conditions impose the boundary conditions. Furthermore, eigenfunctions corresponding to distinct eigenvalues are orthogonal and form a basis for all possible solutions [27]. Here, we invoke the idea of SO(2) symmetry in our system. Due to angular symmetry, the position-dependent part of the Ansatz depends only on the distance from the origin and not the angle, i.e. $\phi(r, \theta) = \phi(r)$. This choice eliminates certain eigenvalues (and their corresponding eigenfunctions) from the solution.

Rewriting the eigenvalue equation in polar coordinates, we obtain

$$r^2\phi''(r) + r\phi'(r) + \frac{\mu^2}{D}r^2\phi(r) = 0, \tag{11}$$

which has the general solution

$$\phi(r) = J_0\left(\frac{\mu}{\sqrt{D}}r\right) + cY_0\left(\frac{\mu}{\sqrt{D}}r\right), \tag{12}$$

where J_n and Y_n are the Bessel functions of the first and second kind of nth order, respectively, and c is a constant which shall be determined using boundary conditions. We are now ready to shape our solution according to the boundary conditions given in (6).

At this point, we shall stress that our solution will be a combination of both J_0 and Y_0. This adds a layer of complexity to the problem, as opposed to many common cases where the origin is in the region of interest. If a solution should exist at the origin, one can immediately set $c = 0$, as $Y_0(x)$ diverges as $x \to 0$. In our initial value problem, this is not the case and further computation will be required. For now, we shall postpone this computation and consider the special function $\eta_0^s(x)$

$$\eta_0^s(x) = J_0\left(x\right) + c_s Y_0\left(x\right), \tag{13}$$

such that $\eta_0^{'s}(\beta_s) = 0$ and $\eta_0^s(\alpha\beta_s) = 0$, where $\alpha = d_0/R$ (from now on called the aspect ratio) and $\eta_0^{'s}(x)$ denotes the derivative of $\eta_0^s(x)$ with respect to x. The construction of such a function and the computation method of the set $\{\beta_s\}$ are discussed in detail in Appendix A. We note that $\{\beta_s\}$, called eigenvalues from now on, is an (increasingly) ordered, discrete, and infinite set.

It can be verified through straightforward algebra that the function $\eta_0^s(\beta_s r/R)$ satisfies the two boundary conditions and is a radial solution for the diffusion equation given in (5). Moreover, the following orthogonality condition can be shown to hold for $\eta_0^s(\beta_s x)$:

$$\int_\alpha^1 \eta_0^s(\beta_s x)\eta_0^l(\beta_l x)x \,\mathrm{d}x = \frac{1}{2}\left((\eta_0^s)^2(\beta_s) - \alpha^2(\eta_1^s)^2(\alpha\beta_s)\right)\delta_{sl}, \tag{14}$$

where we simply replace J_0 and Y_0 by J_1 and Y_1 in (13) to find $\eta_1^s(\beta_s x)$.

We find the probability distribution function to be of the form

$$P\left(r,t|r_0\right) = \sum_{s=1}^{\infty} A_s \eta_0^s\left(\beta_s \frac{r}{R}\right) e^{-\beta_s^2 \frac{Dt}{R^2}}, \tag{15}$$

where we note that $\beta_1 > 0$ (see, for example, Table 1 in Appendix B), indicating that for $t \to \infty$ the probability distribution of molecules vanishes everywhere in the space. Taking the orthogonality condition into account, we find the general normalization constants A_s

$$A_s = \frac{1}{\pi R^2}\eta_0^s\left(\beta_s \frac{r_0}{R}\right)\frac{1}{\left((\eta_0^s)^2(\beta_s) - \alpha^2(\eta_1^s)^2(\alpha\beta_s)\right)}, \tag{16}$$

from which we find the solution

$$P\left(r,t|r_0\right) = \sum_{s=1}^{\infty} \frac{\eta_0^s\left(\beta_s \frac{r_0}{R}\right)\eta_0^s\left(\beta_s \frac{r}{R}\right)}{\pi R^2\left((\eta_0^s)^2(\beta_s) - \alpha^2(\eta_1^s)^2(\alpha\beta_s)\right)} e^{-\beta_s^2 \frac{Dt}{R^2}}, \tag{17}$$

where we recall that the set $\{\beta_s\}$ is defined such that $\eta_0^s(\alpha\beta_s) = 0$ and $\eta_0^{'s}(\beta_s) = -\eta_1^s(\beta_s) = 0$ to satisfy the boundary conditions. Now that we have $P\left(r,t|r_0\right)$, we can calculate the hitting rate[2] as

$$n_{hit}(t) = 2\pi d_0 D \frac{\partial P\left(r,t|r_0\right)}{\partial_r}\bigg|_{r=d_0}, \tag{18}$$

where $D\frac{\partial P(r,t|r_0)}{\partial_r}\Big|_{r=d_0}$ represents the probability current into the absorbing receiver. Thus, we find the hitting rate

$$n_{hit}(t) = -2D\sum_{s=1}^{\infty} \frac{\alpha\beta_s\eta_0^s\left(\beta_s \frac{r_0}{R}\right)}{R^2\left((\eta_0^s)^2(\beta_s) - \alpha^2(\eta_1^s)^2(\alpha\beta_s)\right)}\eta_1^s\left(\beta_s\alpha\right) e^{-\beta_s^2 \frac{Dt}{R^2}}. \tag{19}$$

We conclude this section by emphasizing that we are required to find different eigenvalues $\{\beta_s\}$ for each aspect ratio α to construct the special functions $\eta_0^s(x)$ (See Appendix A).

3.2 Verification of Analytic Result and Channel Characteristics

Having found the analytic solution for the 2-D annular channel, we shall now focus on verifying our findings through comparison with particle-based simulations and then discuss the effects of a reflecting boundary on the channel response. In this section, we simulate the hitting rate $n_{hit}(t)$ for different aspect ratios $\alpha = \frac{d_0}{R}$ and interpret certain channel characteristics.

In our simulations, we take the radius of the outer cylinder as $R = 100\mu m$, unless otherwise stated, and simulate the system for different receiver radii d_0 by changing $\alpha = \frac{d_0}{R}$. Changing the diffusion coefficient only re-scales time, which does not affect the correctness of the comparison. For simplicity, we set $D = 80\ \mu m^2/s$ for our illustrations. Unless otherwise stated, simulations are performed with 10^6 particles, and the reflections are performed according to the rollback mechanism, which is discussed in [20].

Now that we have both our analytic solution and the simulation framework, we shall compare the hitting rate, $n_{hit}(t)$, for different aspect ratios α, and different initial positions r_0, in Figure 2. As can be seen from the figure, the simulation and the analytic results are in agreement for multiple scenarios, as expected. In these illustrations, we truncate the analytic result, given in (19), after the $350th$ term. This is possible as the terms in the sum are exponentially suppressed for larger β_s values. In fact, we can choose a parameter β_{s_c} such that

$$\exp\left(-\beta_{s_c}^2 \frac{Dt}{R^2}\right) \ll 1, \tag{20}$$

[2] This quantity is also known as first-passage time probability density distribution in the literature. We occasionally use the term “hitting number” to describe this quantity as well.

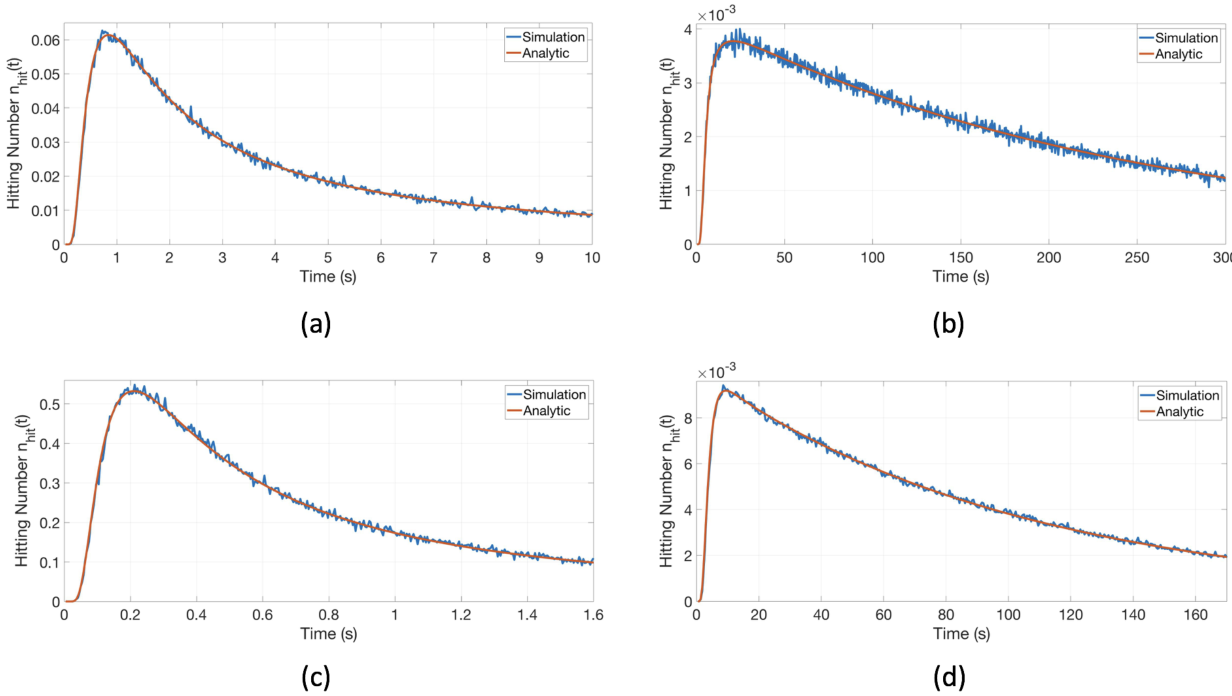

Figure 2: Simulations of hitting rate $n_{hit}(t)$ versus time for $D = 80\mu m^2/s$, $R = 100\mu m$, $d_0 = 1\mu m$ (a,b) and $d_0 = 10\mu m$ (c,d), $r_0 = 20\mu m$ (a,c) and $r_0 = 70\mu m$ (b,d). Note the correspondence between the analytic solution and the simulation in each case. We use 350 terms when finding the analytic result for $n_{hit}(t)$.

where t is the final time of interest and truncate the series afterward. In order to visualize the relative contribution of each term in the summation, we first define a time period of interest $[\Delta t, 10t_\gamma]$, where Δt is the smallest time possible to detect a signal and

$$t_\gamma = \frac{(r_0 - d_0)^2}{D} \tag{21}$$

is the scale-free time of the channel such that $[\Delta t, 10t_\gamma]$ includes several factors of the characteristic time of the diffusion process for any set of r_0, d_0 and D. Therefore, for each set of parameters, a new t_γ is calculated. For the truncation analysis, we set $\Delta t = t_\gamma/1000$.

Having defined the time of interest, we can find the relative contribution of each term in the summation as

$$f_s = \frac{-2\frac{\alpha\eta_0^s\left(\beta_s\frac{r_0}{R}\right)}{\beta_s\left((\eta_0^s)^2(\beta_s)-\alpha^2(\eta_1^s)^2(\alpha\beta_s)\right)}\eta_1^s\left(\beta_s\alpha\right)\left(e^{-\beta_s^2\frac{D\Delta t}{R^2}} - e^{-\beta_s^2\frac{Dt_\gamma}{R^2}}\right)}{\int_{\Delta t}^{t_\gamma}\mathrm{d}t\, n_{hit}(t)}, \tag{22}$$

such that $\sum_{s=1}^{\infty} f_s = 1$. Furthermore, we define the cumulative contribution as

$$F_s = \sum_{r=1}^{s} f_r. \tag{23}$$

We show the relative contribution of each term in the summation and their cumulative behavior for the time period $[\Delta t, 10t_\gamma]$ in Fig. 3. As can be seen from the figure, the initial position of the transmitter is of high importance for the most efficient truncation. This can be understood by the exponential suppression of higher index terms for later times, as $\exp\left(-\beta_s^2\frac{Dt_\gamma}{R^2}\right)$ becomes more negligible for large t_γ, which is the case for large r_0 values. This also justifies the choice of the upper-bound, $10t_\gamma$, for the time of interest, as later times can already be described by the terms, which one picks when describing earlier times. For many cases, the most efficient truncation (at term $s = s_c$) can be performed by considering the difference between the absolute relative contribution of the two consequent terms such that $||f_{s_c+1}| - |f_{s_c}|| \ll \epsilon$, where ϵ is a small positive number. An equivalent method is to consider $|1 - |F_{s_c}|| \ll \epsilon$ and then to choose the cut-off s_c accordingly, since F_s is unit-normalized for $s \to \infty$ by definition. For cases where computing $\{\beta_s\}$ becomes costly, the most efficient truncation method discussed here can be easily implemented. Fortunately, the channel impulse response discussed in this letter allows finding a large number of $\{\beta_n\}$ very efficiently. Hence, for the entirety of the letter, analytic results in each applicable figure are computed using more than 300 terms.

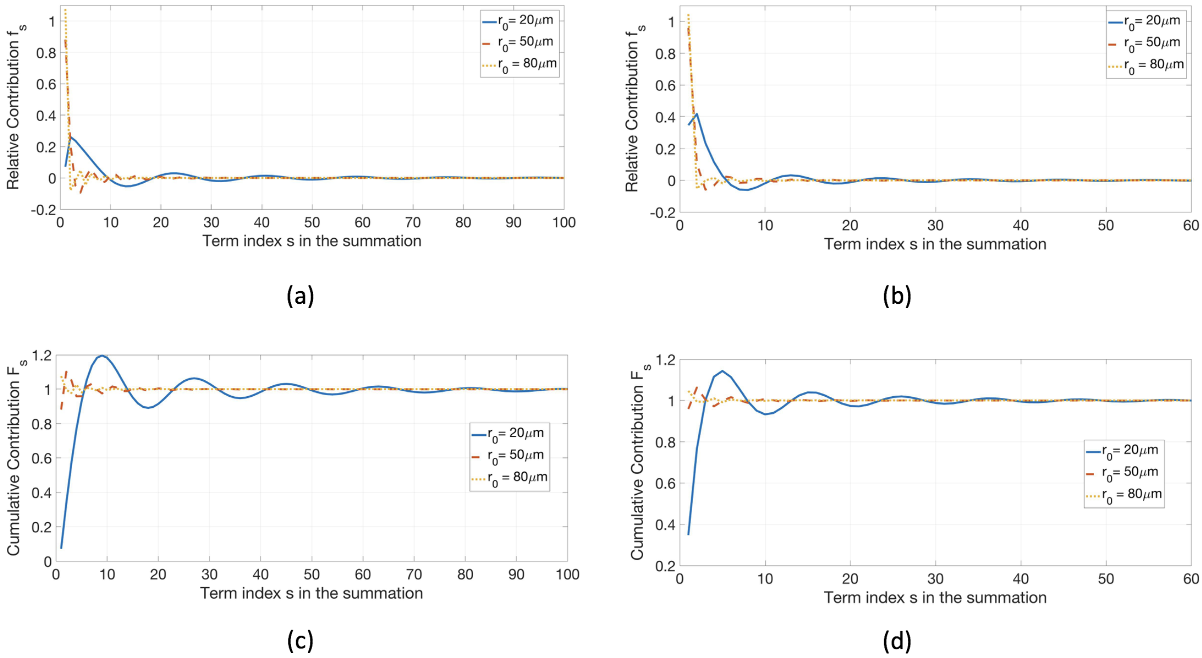

Figure 3: Relative contribution f_s and cumulative contribution F_s for finite number of terms in (19) for $R = 100\mu m$, $d_0 = 10\mu m$ (a)-(c) and $d_0 = 1\mu m$ (b)-(d).

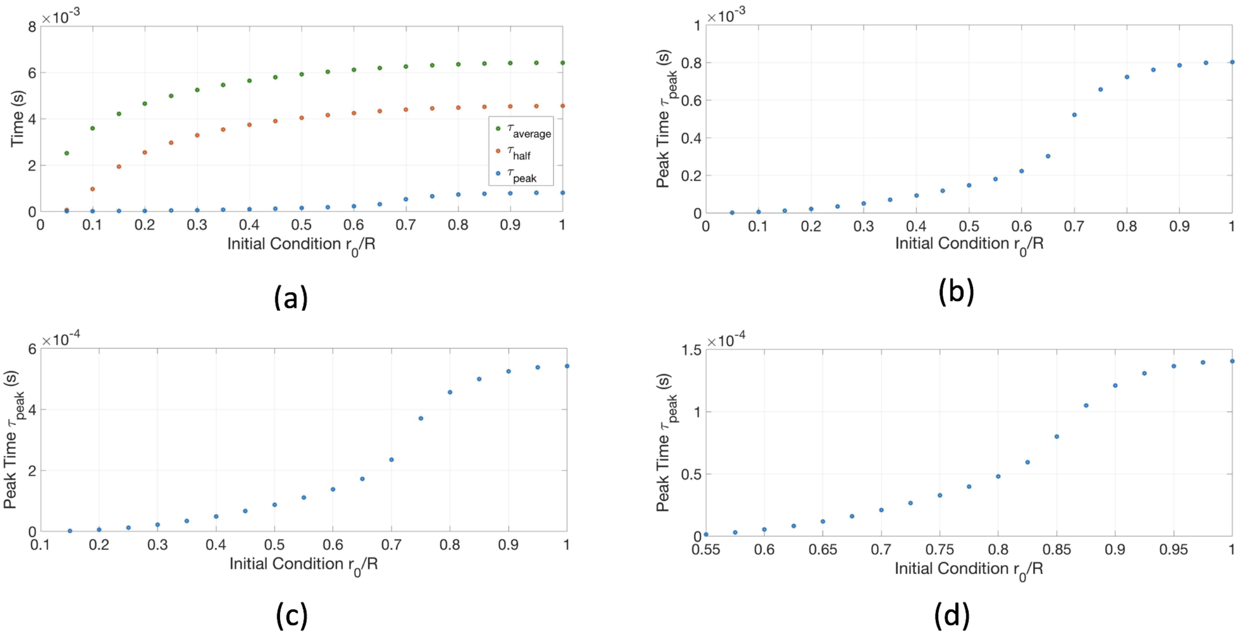

Figure 4: The channel characteristic times ($\tau_{average}$, τ_{half} and τ_{peak}) for $\alpha = 0.01$ (a), the peak time behavior versus initial condition, r_0, for $\alpha = 0.01$ (b), $\alpha = 0.1$ (c) and $\alpha = 0.5$ (d). Note the apparent trend change for τ_{peak} once the initial release point $(r_0 - d_0) \simeq \frac{2}{3} l_c$, where $l_c = R - d_0$ is the channel length. This is due to molecules reflecting from the boundary being dominant for the absorption. For closer initial release points r_0, the peak time vs. initial distance scales as $\tau_{peak} \sim (r_0 - d_0)^2$ in agreement with the 3-D spherical receiver point transmitter case [14]. The channel characteristics are calculated and illustrated for $R = 500nm$ and $D = 80\mu m^2/s$. Due to inherent space scaling symmetry, the shape of the curves are the same for micro-scales as well, within a scaling of time. We use more than 300 terms (different for each α) in the summation for the analytic result while computing the channel characteristic times.

Now, we can focus on the channel performance, specifically effects caused by the existence of the reflecting boundary. First we define some useful concepts:

Definition 1 (Peak time) *The peak time τ_{peak} is defined in [14] as the time such that the hitting rate is maximum, e.g.*

$$\frac{\partial n_{hit}(t)}{\partial t}\Big|_{t=\tau_{peak}} = 0. \tag{24}$$

Definition 2 (Average time) *The average time $\tau_{average}$ is defined as the expected value of the time where the hitting rate $n_{hit}(t)$ is taken to be the probability density function, i.e.,*

$$\tau_{average} = \int_0^{\infty} t\, n_{hit}(t)\, \mathrm{d}t. \tag{25}$$

Note that the hitting rate being the probability density function for time is a direct consequence of the continuity equation.

Definition 3 (Half time) *The half time τ_{half} is defined as the time it takes for the molecule to be absorbed with a probability of* 0.5*, i.e.,*

$$\int_0^{\tau_{half}} n_{hit}(t)\, \mathrm{d}t = 0.5. \tag{26}$$

Many of the 2-D annular channel characteristics and the effects of the boundary on the channel can be captured through the peak, average, and half-time values and their dependence on the initial release point r_0. An illustration of these parameters is shown in Fig. 4.

The importance of peak time, τ_{peak}, in communication aspects has been discussed in [14]. As an addition, we believe that both $\tau_{average}$ and τ_{half} can be useful when characterizing the channel. Most importantly, τ_{half} could be used as a reliable measure when defining sampling time for communication purposes, as one requires to sample at least more than half of the messenger molecules to have a signal-to-inter-signal-interference ratio higher than 1. Unfortunately, determining τ_{half} has high computational cost, and therefore a measure, which is easy to compute, is required. Fortunately, $\tau_{average}$ has similar behavior and is within the same order of magnitude of τ_{half} while having an easy-to-compute analytic expression. Moreover, comparing τ_{peak} with τ_{half} and $\tau_{average}$, we can qualitatively infer the importance of tail effects in a 2-D channel. The difference between these quantities shows the relative contribution that comes from the tail of $n_{hit}(t)$ for $t \geq \tau_{peak}$ with respect to earlier times. If most of the molecules arrive at the receiver at early times close to τ_{peak}, we expect the quantity $|\tau_{average} - \tau_{peak}|/\tau_{peak}$ to be of the order unity. Nonetheless, there is an order of magnitude difference between τ_{peak} and $\tau_{average}$ as can be seen from the Fig. 4(a). Hence, tail effects are highly dominant in a 2-D geometry, meaning that a communication process taking place in 2-D should include sampling of messenger molecules for times much larger than τ_{peak}. Moreover, Fig. 4(a) illustrates that τ_{peak} and $\tau_{average}$ have similar behavior versus r_0, where both measures are dominated by the effects due to boundary.

The effect of the reflecting boundary at early times, $\sim O(t_\gamma)$, can best be seen from the peak time τ_{peak}, which is plotted for three different aspect ratios α in Fig. 4(b),(c),(d) for illustration purposes. As is apparent from the figure, the shape of the plot, τ_{peak} vs r_0, depends solely on the initial condition R_0 and is independent of α, hence d_0 and R. When the molecule is initially close to the receiver, the effect of the boundary at early times is negligible and we observe a square-law dependence between the distance and the peak-time τ_{peak}, as was the case for a 3-D spherical receiver and a point transmitter [14]. As we shall see in section 4.2, the unbounded channel can be described by the analytic expression for the bounded channel for $t \in [0, \tau_{peak}]$ in this region. Defining the channel length $l_c = R - d_0$, we realize that the deviation from the square-law is apparent when the release distance is $(r_0 - d_0) \simeq \frac{2}{3} l_c$. This $(r_0 - d_0)$ is indeed the critical distance, after which the boundary effects become dominant at time scales $t \simeq \tau_{peak}$. The same transition is not as apparent with τ_{half} and $\tau_{average}$ due to the following reason: the existence of the reflecting boundary ensures that the molecules are absorbed earlier than in the unbounded case, hence the effect of the boundary on τ_{half} and $\tau_{average}$ is present even when the molecule is initially very far away from the boundary or close to the receiver.

Considering that there are infinitely many summed terms in the expression for $n_{hit}(t)$, it is not straightforward to obtain a formula for τ_{peak} and τ_{half}. Fortunately, one can find an analytic expression for the average time:

$$\tau_{average} = -2 \sum_{s=1}^{\infty} \frac{\alpha R^2 \eta_0^s \left(\beta_s \frac{r_0}{R}\right) \eta_1^s (\alpha \beta_s)}{D \beta_s^3 \left((\eta_0^s)^2(\beta_s) - \alpha^2 (\eta_1^s)^2(\alpha\beta_s)\right)}. \tag{27}$$

While finding this expression we exchange the integral and the sum, therefore, we shall present a proof of concept for the convergence of this expression. In order to do so, we first define an estimate for $\tau_{average}$ as

$$\tau_{average}^{est}(t) = \int_0^t n_{hit}(\tau) \tau\, \mathrm{d}\tau, \tag{28}$$

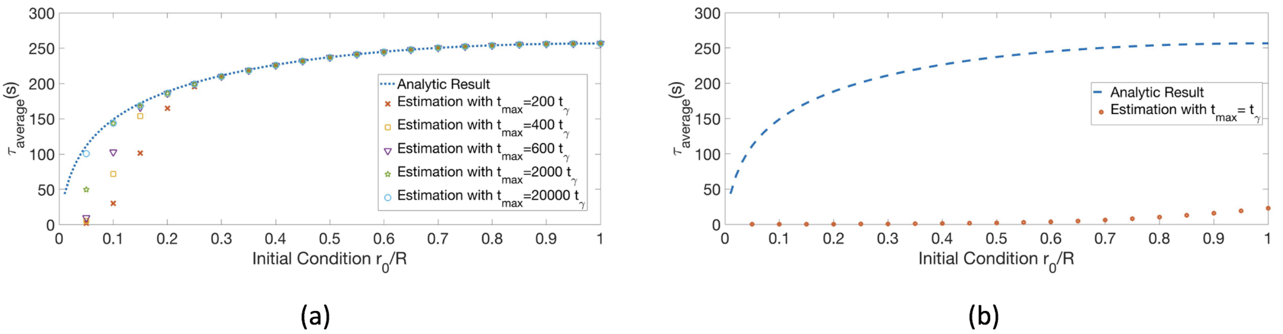

Figure 5: Comparison of $\tau_{average}$ and $\tau^{est}_{average}(t_{max})$ for $d_0 = 1\mu m$, $R = 100\mu m$, $D = 80\mu m^2/s$ and various t_{max} versus r_0/R (a), for $t_{max} = t_\gamma$ versus r_0/R (b). All analytic results are calculated using 350 terms.

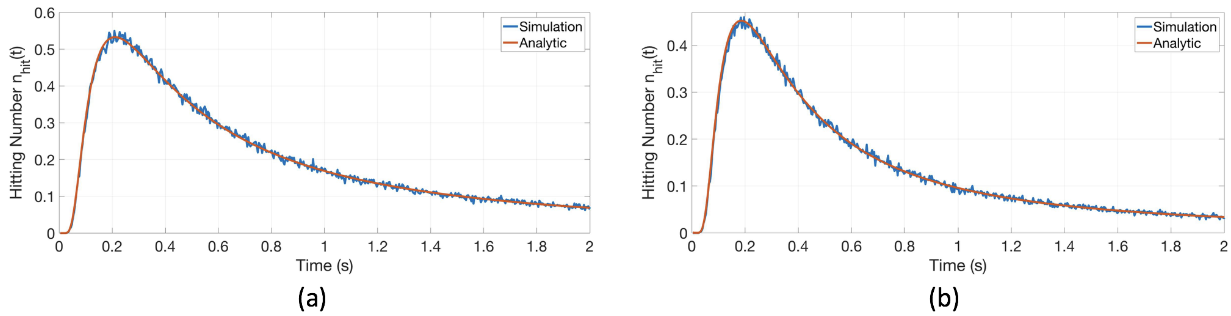

Figure 6: Comparison of simulation and angular-dependent analytic result of $n_{hit}(t)$ for $R = 100\mu m$, $d_0 = 10\mu m$, $r_0 = 20\mu m$, $D = 80\mu m^2/s$, $\theta_f = \pi/2$ (a) and $\theta_f = \pi/6$ (b). Comparing with Fig. 2(c), one can see that for $r_0 = 20\mu m$ almost all particles hit inside the angle range $[-\pi/2, \pi/2]$. We use 4×10^6 terms when obtaining the angular-dependent analytic result.

where $\lim_{t\to\infty} \tau^{est}_{average}(t) = \tau_{average}$. We compare the estimate with the analytic expression in Fig. 5(a) for various final times t_{max} versus r_0/R. As can be seen from the figure, the estimate converges to the analytic result. This is expected, since in (27) the terms in the summation behave as $\sim 1/\beta_s^3$ for large indices and are suppressed accordingly.

We note that the similar behavior of τ_{half} and $\tau_{average}$ is not surprising at all. We already illustrated this similarity in Fig. 4(a), but this result can be considered more general due to the scale invariance of $n_{hit}(t)$ as long as tail effects are dominant. One way to see this scale invariance is to consider (19), where $n_{hit}(t)$ depends dominantly on the parameter α and r_0/R as long as $t \geq O(\tau_{peak})$ or equivalently $t \geq O(t_\gamma)$. Therefore, as long as times $t \geq t_\gamma$ have more dominant effects on $\tau_{average}$, we can expect similar behavior for both $\tau_{average}$ and τ_{half}. Finally, we plot $\tau_{average}$ and $\tau^{est}_{average}(t_\gamma)$ versus initial condition r_0 in Fig. 5(b) to show that earlier times, $t \leq t_\gamma$, have negligible contributions for $\tau_{average}$. Therefore, as t_γ/τ_{peak} is of ~~the~~ order unity, the tail effects are indeed dominant when determining $\tau_{average}$.

4 Applications to Various Channels

Having characterized the 2-D annular channel, we now perform comparisons with particle based simulations to illustrate that the impulse response can be used for different types of channels under certain conditions. In addition, we show that with a similar approach, we can also find the angle-dependent impulse response for the 2-D annular channel.

4.1 2-D Annular Channel: Angular Dependent Impulse Response

Inspired from the nature of diffusion, it has been shown that using a partially-counting receiver based on angular position has beneficial effects in molecular communication [28]. Since molecules move slowly, it takes much higher expected time to move to the part of the receiver that is far from the transmitter. These parts can also be represented by the reception angle as shown in Fig. 1(c). In addition, angle-dependent channel impulse response can be used to improve the channel performance by reducing inter symbol interference as proposed in [28].

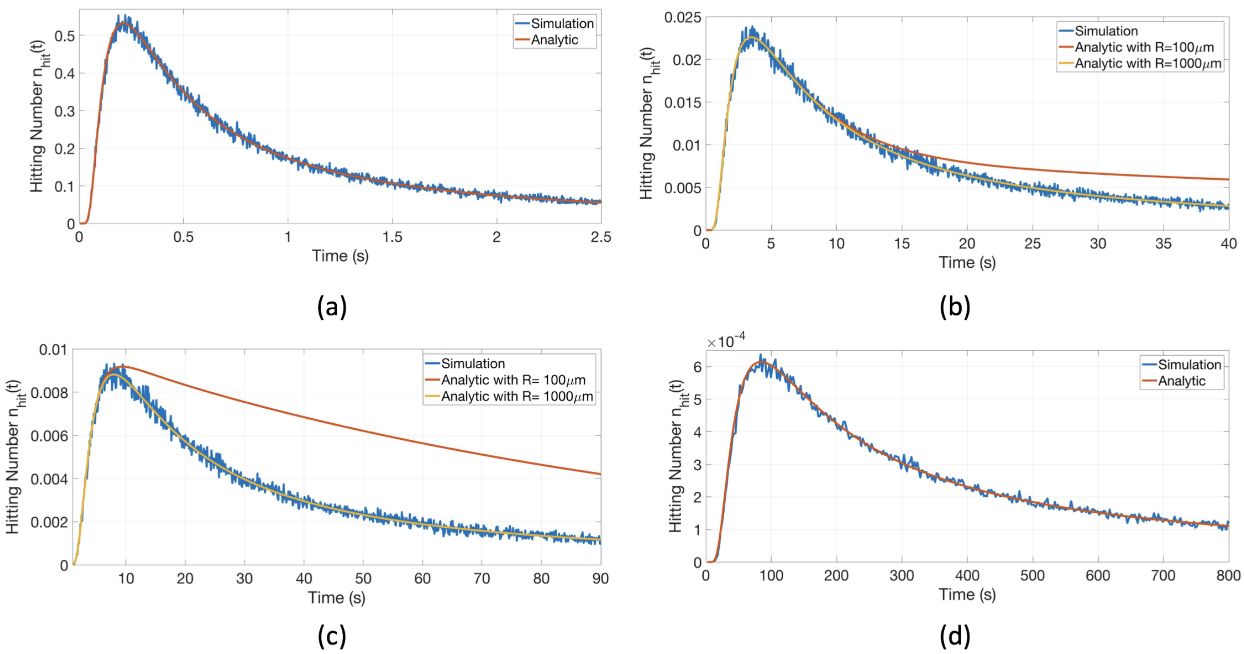

Figure 7: Comparison of Simulation and Analytic Estimations for unbounded channel for $\alpha = 0.1$ and $r_0 = 20\mu m$ (a), for $\alpha = 0.1\&0.01$ and $r_0 = 50\mu m$ (b), for $\alpha = 0.1\&0.01$ and $r_0 = 70\mu m$ (c), for $\alpha = 0.01$ and $r_0 = 200\mu m$ (d). For all simulations, $d_0 = 10\mu m$ and $D = 80\mu m^2/s$, whereas R changes in each subfigure according to $\alpha = d_0/R$.

The receiver (in Fig. 1(c)) absorbs all the molecules upon collision, but counts only those that arrive inside the angular interval $[-\theta_f, \theta_f]$ and disregards the rest. We can modify our previous calculations to find an analytic solution for this case as well, which is carried out in Appendix B.

For this channel, we define the hitting rate as the probability of a single released molecule to hit the receiver inside the angle range $[-\theta_f, \theta_f]$ between times t and $t + \mathrm{d}t$

$$n_{hit}(\theta_f, t) = \int_{-\theta_f}^{\theta_f} Dd_0 \left(\frac{\partial}{\partial r} P(r, \theta, t) \right) \Bigg|_{r=d_0} \mathrm{d}\theta. \tag{29}$$

From (B.10), we find the hitting rate as (For definitions, see Appendix B)

$$\begin{aligned} n_{hit}(\theta_f, t) = &\sum_{s=1}^{\infty} \frac{\theta_f D \alpha \beta_{0s}}{\pi R^2 I_{0s}} \eta_0^s \left(\beta_{0s} \frac{r_0}{R} \right) \eta_0'^s \left(\beta_{0s} \frac{d_0}{R} \right) e^{-\beta_{0s}^2 \frac{Dt}{R^2}} \\ &+ \sum_{p=1}^{\infty} \sum_{s=1}^{\infty} \frac{2D\alpha\beta_{ps}}{p\pi R^2 I_{ps}} \sin(p\theta_f) \eta_p^{ps} \left(\beta_{ps} \frac{r_0}{R} \right) \eta_p'^{ps} \left(\beta_{ps} \frac{d_0}{R} \right) e^{-\beta_{ps}^2 \frac{Dt}{R^2}}. \end{aligned} \tag{30}$$

A comparison of analytic and simulation results for this channel type is given in Fig. 6. For the remainder of this letter, we focus on the receiver type with $\theta_f = \pi$, for which (30) reduces to (19).

4.2 2-D Unbounded Channel: An Analytic Approximation

The impulse response for the 2-D unbounded channel with an absorbing receiver has been missing from the literature, whereas the impulse responses for 1-D and 3-D channels are well-known [14, 6]. Fortunately, our derivations for the 2-D annular channel can be utilized to estimate the impulse response for the 2-D unbounded channel with an arbitrarily small error. The trade-off for obtaining an arbitrarily small error is the computational complexity, as more β_s terms will be required in (19) to describe the channels with smaller aspect ratios α. This is due to the fact that as $\alpha \to 0$, the eigenvalues β_s become closer and closer. Therefore, it is not trivial to obtain an exact analytic result in the limit $\alpha \to 0$, since this would require integrating an integrand, which has combinations of various Bessel functions both in its numerator and denominator and has infinitely many poles. Therefore, we shall focus on making accurate estimations for the 2-D unbounded channel while confirming our observations regarding the effects of the boundary on τ_{peak} from section 3.2.

In Fig. 7, simulation results for the 2-D unbounded channel and corresponding analytic estimates are illustrated. As is apparent from the figure, as long as the boundary R is sufficiently far away, the analytic

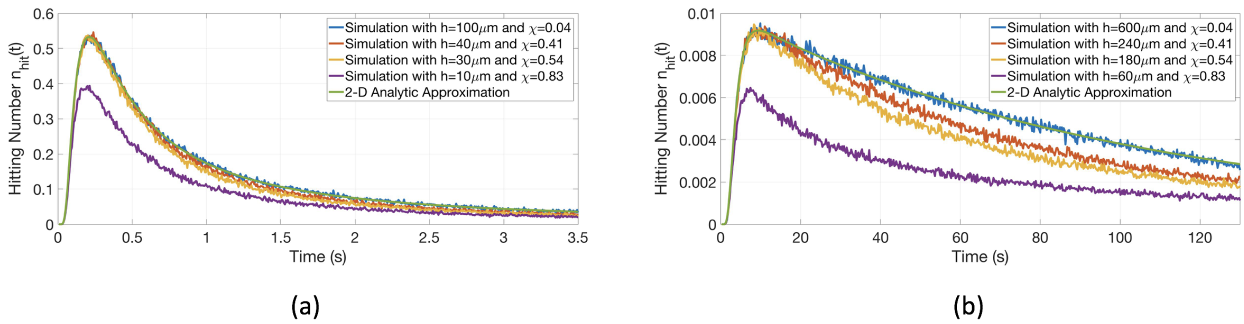

Figure 8: Comparison of Simulation and Analytic Estimations for the 3-D channel with $R = 100\mu m$, $d_0 = 10\mu m$, $D = 80\mu m^2/s$, the boundary height $h_b \to \infty$ and various receiver heights h for $r_0 = 20\mu m$ (a) and for $r_0 = 70\mu m$ (b). χ values are evaluated with $t_{max} = 3.75$s for (a) and with $t_{max} = 135$s for (b). 350 terms are used when obtaining the analytic estimate in each case.

estimate matches the simulations quite well. In fact, from our discussion on τ_{peak}, we expect that the boundary effects on the peak-time will be apparent when $(r_0 - d_0) \simeq \frac{2}{3} l_c$. This is certainly the case for Fig. 7(c), where the analytic estimate with $R = 100\mu m$ diverges from the simulation around the peak position. In this case, simply increasing the boundary radius $R \to 1000\mu m$ results in an estimate that matches the simulations well. We can infer from the simulations that choosing the boundary radius R according to $(r_0 - d_0) \simeq 0.2$ results in a good-agreement between the simulation and the analytic estimate for the time of interest $t \in [0, O(t_\gamma)]$.

Fig. 7(b) illustrates the strong influence of the boundary on τ_{half} and $\tau_{average}$, as the analytic estimate with $R = 100\mu m$ does not match the tail of the simulation. Even though τ_{peak} matches in this case, the increase in the tail results in molecules being absorbed earlier than in the unbounded case. This leads to the saturation effect we observe in Fig. 4(a) for τ_{half} and $\tau_{average}$ for larger r_0/R values. Thus, we see once more that τ_{peak} alone is not sufficient to describe the characteristics of the 2-D bounded channel.

4.3 3-D Channel: Comparison with Simulations

Now, we turn to estimating the impulse response for the 3-D channel with coaxial cylinders, as depicted in Fig. 1(a). In section 2, we discussed a simplified assumption such that the 3-D channel can be approximated by the 2-D annular channel. Now, we shall perform comparisons with particle based simulations to verify our findings.

For now, we will revisit (4) and re-write it, for simplicity, as follows

$$\chi = 2Q\left(\frac{h}{2\sqrt{2Dt_{max}}}\right) \implies \chi < \epsilon, \tag{31}$$

where ϵ is our crude over-estimate of the error-bound and t_{max} is the maximum time of interest. For illustration purposes, we shall consider the most extreme case, where the boundary height $h_b \to \infty$ and the receiver height is $h = 2h_0$. The transmitter is located in the middle as in Fig. 1. The comparison is shown in Fig. 8 for two different initial conditions $r_0 = 20\mu m$ and $r_0 = 70\mu m$. As can be seen from the figure, χ is indeed an over-estimate, since the analytic estimate follows the simulations even for high χ values.

As can be seen from Fig. 8(b), the discrepancy between the analytic estimate and the simulations becomes more apparent for large r_0/R values, as the tail effects become important at earlier times and more particles arrive at the receiver until the time of interest, amplifying the existing error correspondingly. For the usual time of interest, $t \in [0, O(t_\gamma)]$, the analytic estimate matches the simulations if $h = 10(r_0 - d_0)$ very well. We can also see this from our crude estimate by setting $t_{max} = \kappa t_\gamma$ and $h = 10(r_0 - d_0)$:

$$\chi = 2Q\left(\frac{h}{2\sqrt{2D\kappa t_\gamma}}\right) = 2Q\left(\frac{5}{\sqrt{2\kappa}}\right). \tag{32}$$

For example, this function yields 0.04 for $\kappa = 3$ and 0.15 for $\kappa = 6$. Both cases are acceptable since this is a crude overestimate of the upper-bound on the error.

5 Conclusion

In this work, we derived the impulse response of the 2-D annular channel first for SO(2) symmetric initial conditions, then broke the symmetry while offering a more rigorous and angle-dependent description for the impulse response inside the channel. In this pursuit, we defined a special function $\eta_0^s(x)$ (or $\eta_p^{ps}(x)$ in general), which is a combination of Bessel functions of the first and second kind. This function satisfies the necessary boundary conditions and is an exact solution to the radial part of the diffusion equation under separation of variable Ansatz. This method of obtaining an impulse response leads to an infinite number of terms, the sum of which converges for $t > 0$. It is shown that the infinite sum in the analytic solution can be truncated after a certain number of terms depending on the time interval one is interested in. Furthermore, we show the agreement between the Monte-Carlo simulations and the analytic solutions for different channel and receiver parameters, such as the aspect ratio α, the boundary radius R, and the receiver radius d_0. This equivalence constitutes the evidence for the accuracy of our findings.

Having verified our findings, we explore the dependency of certain channel characteristics on the initial position of the transmitter. Regarding the peak time τ_{peak} simulations, the effect of the boundary on the peak time is more apparent as the initial position of the transmitter is around $2l_c/3$, where $l_c = R - d_0$ is the channel length. As $r_0 > l_c$, there is an apparent shift in the peak time, caused by the boundary. Nonetheless, this trend shift is not apparent for the average and half time, $\tau_{average}$ and τ_{half}. The intuitive reason behind this phenomenon can be explained through the tail effect. The average and half time values are more dependent on the existence of the boundary as they rely not only on the peak of the hitting rate, but also on the behavior of the tail that follows the peak. As the transmitter is placed further from the receiver, the contribution from the tail surpasses greatly the contribution from the peak, hence smoothing out the distinct trend shift for $r \simeq 2l_c/3$. Evidence for this phenomenon can be observed from the relatively large values of average and half times compared to lower values of the peak times, as the difference between τ_{peak} and $\tau_{average}/\tau_{half}$ depicted in Fig. 4 is approximately an order of magnitude. Moreover, we present an analytic expression for $\tau_{average}$, which can be extremely useful when choosing a sampling time for the receiver in a communication scenario.

Finally, we used our findings to describe the impulse response of various channels: the angular-dependent response of the 2-D annular channel, an analytic estimate for the 2-D unbounded channel and finally an analytic approximation for the 3-D diffusion channel consisting of a cylindrical receiver and reflecting boundary. Since no exact analytic result exists in the literature, our findings constitute a leap forward in understanding the impulse response of the 2-D unbounded channel. As a future work, we plan to explore the angular dependent impulse response of the 2-D annular channel and the corresponding channel characteristics, as well as possible applications to many transmitter communications.

Acknowledgements

Research at the Perimeter Institute is supported by the Government of Canada through the Department of Innovation, Science and Economic Development Canada, and by the Province of Ontario through the Ministry of Research and Innovation. Fatih Dinc would like to thank Leander Thiele for commenting on the manuscript and pointing towards important references in the diffusion literature. The work of A.E. Pusane and T. Tugcu was partially supported by the State Planning Organization (DPT) of Turkey under the project TAM (2007K120610).

References

[1] C. Chevalier, O. Bénichou, B. Meyer, and R. Voituriez, "First-passage quantities of brownian motion in a bounded domain with multiple targets: a unified approach," *Journal of Physics A: Mathematical and Theoretical*, vol. 44, no. 2, p. 025002, 2010.

[2] C. Mejía-Monasterio, G. Oshanin, and G. Schehr, "First passages for a search by a swarm of independent random searchers," *Journal of Statistical Mechanics: Theory and Experiment*, vol. 2011, no. 06, p. 06022, 2011.

[3] S. N. Majumdar, A. Rosso, and A. Zoia, "Hitting probability for anomalous diffusion processes," *Physical review letters*, vol. 104, no. 2, p. 020602, 2010.

[4] S. Condamin, O. Bénichou, V. Tejedor, R. Voituriez, and J. Klafter, "First-passage times in complex scale-invariant media," *Nature*, vol. 450, no. 7166, p. 77, 2007.

[5] T. G. Mattos, C. Mejía-Monasterio, R. Metzler, and G. Oshanin, "First passages in bounded domains: When is the mean first passage time meaningful?" *Physical Review E*, vol. 86, no. 3, p. 031143, 2012.

[6] S. Redner, *A Guide to First-passage Processes.* Cambridge UK: Cambridge University Press, 2001.

[7] I. F. Akyildiz, F. Brunetti, and C. Blázquez, "Nanonetworks: A new communication paradigm," *Computer Networks*, vol. 52, no. 12, pp. 2260–2279, 2008.

[8] I. F. Akyildiz, M. Pierobon, S. Balasubramaniam, and Y. Koucheryavy, "The internet of bio-nano things," *IEEE Communications Magazine*, vol. 53, no. 3, pp. 32–40, March 2015.

[9] N. Farsad, H. B. Yilmaz, A. Eckford, C.-B. Chae, and W. Guo, "A comprehensive survey of recent advancements in molecular communication," *IEEE Commun. Surveys Tuts.*, vol. 18, no. 3, pp. 1887–1919, 2016.

[10] T. Nakano, M. J. Moore, F. Wei, A. V. Vasilakos, and J. Shuai, "Molecular communication and networking: Opportunities and challenges," *IEEE Transactions on NanoBioscience*, vol. 11, no. 2, pp. 135–148, June 2012.

[11] D. Malak and O. B. Akan, "Molecular communication nanonetworks inside human body," *Nano Communication Networks*, vol. 3, no. 1, pp. 19–35, 2012.

[12] A. Noel, K. Cheung, and R. Schober, "Improving receiver performance of diffusive molecular communication with enzymes," *IEEE Trans. NanoBiosci.*, vol. 13, no. 1, pp. 31–43, Mar. 2014.

[13] A. W. Eckford, "Nanoscale communication with Brownian motion," in *CISS'07. 41st Annual Conference on Information Sciences and Systems, 2007.* IEEE, 2007, pp. 160–165.

[14] H. B. Yilmaz, A. C. Heren, T. Tugcu, and C.-B. Chae, "Three-dimensional channel characteristics for molecular communications with an absorbing receiver," *IEEE Communications Letters*, vol. 18, no. 6, pp. 929–932, 2014.

[15] B. C. Akdeniz, A. E. Pusane, and T. Tugcu, "2-D channel transfer function for molecular communication with an absorbing receiver," in *2017 IEEE Symposium on Computers and Communications (ISCC).* IEEE, 2017, pp. 938–942.

[16] D. L. L. Dy and J. Esguerra, "First-passage-time distribution for diffusion through a planar wedge," *Physical Review E*, vol. 78, no. 6, p. 062101, 2008.

[17] G. Genc, Y. E. Kara, T. Tugcu, and A. E. Pusane, "Reception modeling of sphere-to-sphere molecular communication via diffusion," *Nano communication networks*, vol. 16, pp. 69–80, 2018.

[18] A. Noel, D. Makrakis, and A. Hafid, "Channel impulse responses in diffusive molecular communication with spherical transmitters," *in Proc. CSIT Biennial Symposium on Communications Jun. 2016*, 2016.

[19] L. P. Giné and I. F. Akyildiz, "Molecular communication options for long range nanonetworks," *Computer Networks*, vol. 53, no. 16, pp. 2753–2766, 2009.

[20] M. Turan, M. . Kuran, H. B. Yilmaz, I. Demirkol, and T. Tugcu, "Channel model of molecular communication via diffusion in a vessel-like environment considering a partially covering receiver," in *2018 IEEE International Black Sea Conference on Communications and Networking (BlackSeaCom)*, June 2018, pp. 1–5.

[21] W. Wicke, T. Schwering, A. Ahmadzadeh, V. Jamali, A. Noel, and R. Schober, "Modeling duct flow for molecular communication," in *GLOBECOM 2018-2018 IEEE Global Communications Conference.* IEEE, 2018.

[22] A. O. Bicen and I. F. Akyildiz, "System-theoretic analysis and least-squares design of microfluidic channels for flow-induced molecular communication," *IEEE Transactions on Signal Processing*, vol. 61, no. 20, pp. 5000–5013, 2013.

[23] Y. Sun, K. Yang, and Q. Liu, "Channel capacity modelling of blood capillary-based molecular communication with blood flow drift," in *Proceedings of the 4th ACM International Conference on Nanoscale Computing and Communication.* ACM, 2017, p. 19.

[24] F. Dinc, B. C. Akdeniz, A. E. Pusane, and T. Tugcu, "Impulse response of the channel with a spherical absorbing receiver and a spherical reflecting boundary," *arXiv preprint arXiv:1804.03383*, 2018.

[25] M. M. Al-Zubi and A. S. Mohan, "Modeling of ligand-receptor protein interaction in biodegradable spherical bounded biological micro-environments," *IEEE Access*, vol. 6, pp. 25 007–25 018, 2018.

[26] R. B. Guenther and J. W. Lee, *Partial differential equations of mathematical physics and integral equations.* Courier Corporation, 1996.

[27] D. S. Grebenkov and B.-T. Nguyen, "Geometrical structure of Laplacian eigenfunctions," *SIAM Review*, vol. 55, no. 4, pp. 601–667, 2013.

[28] B. C. Akdeniz, N. A. Turgut, H. B. Yilmaz, C.-B. Chae, T. Tugcu, and A. E. Pusane, "Molecular signal modeling of a partially counting absorbing spherical receiver," *IEEE Transactions on Communications*, 2018.

APPENDIX

A Derivation of $\eta_0^s(\beta_s x)$

When finding the impulse response of the 2-D channel, we have assumed that there exist functions $\eta_0^s(\beta_s x)$ such that $\eta_0^{'s}(\beta_s) = 0$ and $\eta_0^s(\alpha\beta_s) = 0$. In this section, we shall discuss how to construct such functions and illustrate an algorithm to find the eigenvalues ($\{\beta_s\}$).

To begin with, we can rearrange the radial solution slightly (ignoring the general normalization constant for now) as

$$\phi(r) = J_0\left(ar\right) + cY_0\left(ar\right), \tag{A.1}$$

where we define $a \equiv \frac{\mu}{\sqrt{D}}$ for simpler algebra. Using the boundary conditions (6a) and (6b), we find the following set of linear equations:

$$-aJ_1(aR) - caY_1(aR) = 0, \tag{A.2a}$$

$$J_0(ad_0) + cY_0(ad_0) = 0. \tag{A.2b}$$

Rearranging the terms, we can obtain

$$c = -\frac{J_1(aR)}{Y_1(aR)}, \tag{A.3a}$$

$$c = -\frac{J_0(ad_0)}{Y_0(ad_0)}, \tag{A.3b}$$

where setting $aR = \beta$ and $\alpha = \frac{d_0}{R}$, we look for the solutions of the equation

$$\frac{J_1(\beta)}{Y_1(\beta)} - \frac{J_0(\alpha\beta)}{Y_0(\alpha\beta)} = 0, \tag{A.4}$$

which we call the *characteristic equation*. There are infinitely many solutions for this equation, each of which corresponds to a distinct eigenvalue and an eigenfunction of the Laplacian operator. We also note that c is fully determined by the procedure above. Finally, we define the function

$$\eta_0^s(x) = J_0\left(x\right) + c_s Y_0\left(x\right). \tag{A.5}$$

Without a given aspect ratio α, this is the most general function we can define. If α is given, then we can construct a code that finds the roots of the characteristic equation. This is feasible, because the roots become periodic as $\beta \to \infty$. This can be shown by considering the large argument asymptotic behavior of the Bessel functions, where both $J_p(x)$ and $Y_p(x)$ behave as $\sim \cos\big(x - p\frac{\pi}{2} - \frac{\pi}{4}\big)/\sqrt{x}$ and $\sim \sin\big(x - p\frac{\pi}{2} - \frac{\pi}{4}\big)/\sqrt{x}$, respectively. Then, (A.4) becomes a trigonometric equation:

$$\cot\left(\beta - \frac{3\pi}{4}\right) = \cot\left(\alpha\beta - \frac{\pi}{4}\right). \tag{A.6}$$

For small α, such that $\alpha < 0.5$, the shift $\beta \to \beta + \pi$ leaves the left-hand-side (LHS) of this equation invariant while the RHS changes slowly. Then, in the second shift $\beta \to \beta + \pi$, the RHS does not complete a periodic rotation over its range, as $\alpha 2\pi < \pi$, whereas the LHS completes the second periodic rotation. Hence, for $\alpha < 0.5$, the consecutive roots are contained at least within the interval $\beta_{n-1} - \beta_n \in [\pi, 2\pi]$. A similar argument can be made for cases $0.5 < \alpha < 1$. Hence, as $\beta \to \infty$, the roots are contained within periodic intervals, an example of which can be seen in Table 1 for $\alpha = 0.1$.

As $\{\beta_s\}$ depends solely on α, this computation needs to be carried out only once for each α value. Once the roots β_s are found, we can construct the eigenfunctions $\eta_0^s(\beta_s x)$ given in (13) by finding c_s's.

B Derivation of Angle-Dependent Response

To describe the diffusion of the molecule inside the annular region under angle-dependent conditions, we shall find a solution to Fick's Law, satisfying the necessary boundary conditions

$$\frac{\partial P(r,\theta,t)}{\partial r}\Big|_{r=R} = 0, \tag{B.1a}$$

$$P(r,\theta,t)\Big|_{r=d_0} = 0, \tag{B.1b}$$

$$P(r,\theta,0) = \frac{1}{r}\delta(r-r_0)\delta(\theta-\theta_0). \tag{B.1c}$$

We shall start with the separation of variables ansatz

$$P(r,\theta,t) = \phi(r,\theta)T(t), \tag{B.2}$$

which leads to

$$T(t) = Ae^{-\mu^2 t}, \tag{B.3}$$

and

$$\frac{R''}{R} + \frac{R'}{rR} + \frac{\Theta''}{r^2\Theta} = -\frac{\mu^2}{D}, \tag{B.4}$$

where we define $\phi(r,\theta) = R(r)\Theta(\theta)$ and A is the overall normalization factor to be determined by the initial conditions. $R'(r)$ denotes the derivative of $R(r)$ with respect to r. This equation can be transformed into a Bessel differential equation for the radial part if we set

$$\Theta'' = -p^2\Theta \implies \Theta(\theta) = A_p\cos(p\theta) + B_p\sin(p\theta). \tag{B.5}$$

Then, the radial equation becomes

$$r^2R''(r) + rR'(r) + \left(\frac{\mu^2}{D}r^2 - p^2\right)R(r) = 0. \tag{B.6}$$

After proper re-scaling of the independent variable r, we can find the solution as

$$R(r) = J_p\left(\frac{\mu}{\sqrt{D}}r\right) + cY_p\left(\frac{\mu}{\sqrt{D}}r\right). \tag{B.7}$$

Here, we shall define the function $\eta_p^{ps}(x)$ analogously to (13) as

$$\eta_p^{ps}(x) = J_p(x) + c_{ps}Y_p(x) \tag{B.8}$$

such that $\eta_p^{'ps}(\beta_{ps}) = 0$ and $\eta_p^{ps}(\alpha\beta_{ps}) = 0$, where $\alpha = \frac{d_0}{R}$ as usual. Then, $\eta_p^{ps}(\beta_{ps}\frac{r}{R})$ are indeed solutions to the radial equation with the boundary conditions satisfied, where $\beta_{ps} = \frac{R\mu}{\sqrt{D}}$. In general, to find β_{ps}, we shall solve a linear set of equations similar to what we have done for $\eta_0^s(\beta_s x)$.

Before continuing, we shall give the normalization condition for the special function $\eta_p(\beta_{ps}x)$ as

$$\int_\alpha^1 \eta_p^{ps}(\beta_{ps}x)\eta_{p'}^{p's'}(\beta_{p's'}x)x\,\mathrm{d}x = I_{ps}\delta_{pp'}\delta_{ss'}, \tag{B.9}$$

where we note that I_{ps} can be written in terms of linear combinations of Bessel functions of the first and second kind. Without loss of generality, we can set $\theta_0 = 0$ and find the probability density function for the molecules as

$$\begin{aligned} P(r,\theta,t) = &\sum_{s=1}^{\infty}\frac{1}{2\pi R^2 I_{0s}}\eta_0^s\left(\beta_{0s}\frac{r_0}{R}\right)\eta_0^s\left(\beta_{0s}\frac{r}{R}\right)e^{-\beta_{0s}^2\frac{Dt}{R^2}} \\ &+ \sum_{p=1}^{\infty}\sum_{s=1}^{\infty}\frac{1}{\pi R^2 I_{ps}}\cos(p\theta)\eta_p^{ps}\left(\beta_{ps}\frac{r_0}{R}\right)\eta_p^{ps}\left(\beta_{ps}\frac{r}{R}\right)e^{-\beta_{ps}^2\frac{Dt}{R^2}}. \end{aligned} \tag{B.10}$$

Some β_{ps} values are given in Table 1 in the following page while we note that c_{ps} values can be calculated easily by straightforward algebra.

Table 1: β_{ps} values for $\alpha = 0.1$ calculated by our algorithm to be used in (30). β_{0s} values can also be used for the impulse response given in (19).

	s=1	s=2	s=3	s=4	s=5	s=6	s=7	s=8	s=9	s=10	s=11	s=12	s=13
p=0	1.103	4.979	8.554	12.087	15.603	19.111	22.614	26.114	29.612	33.108	36.604	40.099	43.593
p=1	1.879	5.532	8.975	12.422	15.880	19.346	22.818	26.293	29.772	33.253	36.736	40.219	43.704
p=2	3.056	6.724	10.042	13.347	16.677	20.038	23.424	26.831	30.254	33.689	37.133	40.584	44.041
p=3	4.201	8.016	11.353	14.612	17.858	21.118	24.402	27.714	31.054	34.416	37.798	41.195	44.606
p=4	5.318	9.282	12.682	15.967	19.206	22.428	25.650	28.886	32.142	35.423	38.728	42.056	45.404
p=5	6.416	10.520	13.987	17.313	20.576	23.807	27.020	30.227	33.437	36.657	39.894	43.151	46.430
p=6	7.501	11.735	15.268	18.637	21.932	25.184	28.411	31.622	34.823	38.021	41.222	44.431	47.653
p=7	8.578	12.932	16.529	19.942	23.268	26.545	29.791	33.016	36.226	39.426	42.620	45.812	49.006
p=8	9.647	14.116	17.774	21.229	24.587	27.889	31.155	34.397	37.620	40.831	44.031	47.225	50.414
p=9	10.711	15.287	19.005	22.501	25.891	29.219	32.505	35.764	39.002	42.225	45.436	48.637	51.832
p=10	11.771	16.448	20.223	23.761	27.182	30.535	33.842	37.118	40.371	43.607	46.829	50.040	53.243
p=11	12.826	17.600	21.431	25.009	28.461	31.838	35.167	38.460	41.729	44.978	48.211	51.433	54.645
p=12	13.879	18.745	22.629	26.246	29.729	33.131	36.481	39.792	43.075	46.338	49.583	52.816	56.037
p=13	14.928	19.883	23.819	27.474	30.987	34.415	37.784	41.114	44.412	47.688	50.946	54.189	57.420
p=14	15.975	21.015	25.002	28.694	32.237	35.689	39.079	42.426	45.740	49.030	52.299	55.553	58.794
p=15	17.020	22.142	26.178	29.907	33.478	36.954	40.365	43.730	47.059	50.363	53.644	56.909	60.160
p=16	18.063	23.264	27.347	31.112	34.712	38.212	41.643	45.025	48.371	51.687	54.982	58.257	61.518
p=17	19.104	24.382	28.511	32.311	35.940	39.463	42.914	46.314	49.674	53.005	56.311	59.598	62.869
p=18	20.144	25.496	29.670	33.504	37.160	40.707	44.178	47.595	50.971	54.315	57.634	60.932	64.213
p=19	21.182	26.606	30.824	34.691	38.375	41.945	45.436	48.870	52.261	55.619	58.950	62.259	65.550
p=20	22.219	27.712	31.974	35.874	39.585	43.177	46.687	50.139	53.545	56.916	60.260	63.580	66.881
p=21	23.255	28.816	33.119	37.052	40.789	44.403	47.933	51.401	54.823	58.208	61.563	64.895	68.206
p=22	24.289	29.916	34.261	38.225	41.988	45.624	49.173	52.659	56.095	59.494	62.861	66.204	69.525
p=23	25.323	31.014	35.399	39.394	43.183	46.841	50.409	53.911	57.362	60.774	64.154	67.507	70.839
p=24	26.356	32.109	36.533	40.559	44.373	48.053	51.639	55.158	58.624	62.049	65.441	68.806	72.148
p=25	27.387	33.202	37.665	41.721	45.559	49.260	52.865	56.400	59.881	63.320	66.724	70.099	73.451
p=26	28.418	34.293	38.793	42.879	46.742	50.463	54.087	57.638	61.134	64.585	68.001	71.388	74.750
p=27	29.448	35.382	39.919	44.033	47.920	51.663	55.305	58.872	62.382	65.847	69.275	72.672	76.045
p=28	30.478	36.468	41.042	45.185	49.096	52.859	56.518	60.101	63.626	67.104	70.543	73.952	77.334
p=29	31.506	37.553	42.163	46.333	50.268	54.051	57.728	61.327	64.866	68.356	71.808	75.228	78.620
p=30	32.534	38.636	43.281	47.479	51.436	55.239	58.934	62.549	66.102	69.605	73.069	76.499	79.902
p=31	33.562	39.717	44.397	48.622	52.602	56.425	60.137	63.768	67.334	70.851	74.326	77.767	81.179
p=32	34.588	40.797	45.510	49.762	53.765	57.607	61.337	64.982	68.563	72.092	75.579	79.031	82.453
p=33	35.615	41.875	46.622	50.900	54.925	58.787	62.533	66.194	69.789	73.330	76.828	80.291	83.723
p=34	36.641	42.952	47.731	52.036	56.083	59.963	63.727	67.403	71.011	74.565	78.075	81.548	84.990
p=35	37.666	44.028	48.839	53.169	57.238	61.137	64.917	68.608	72.230	75.796	79.317	82.801	86.253
p=36	38.691	45.102	49.945	54.301	58.390	62.308	66.105	69.811	73.446	77.024	80.557	84.051	87.513
p=37	39.715	46.174	51.049	55.430	59.541	63.477	67.290	71.010	74.659	78.250	81.794	85.298	88.770
p=38	40.739	47.246	52.152	56.557	60.689	64.643	68.472	72.207	75.869	79.472	83.027	86.542	90.023
p=39	41.762	48.317	53.253	57.682	61.835	65.807	69.652	73.401	77.076	80.692	84.258	87.783	91.274
p=40	42.785	49.386	54.352	58.806	62.978	66.969	70.829	74.593	78.281	81.908	85.486	89.021	92.521
p=41	43.808	50.454	55.450	59.927	64.120	68.128	72.005	75.782	79.483	83.122	86.711	90.257	93.766
p=42	44.830	51.521	56.546	61.047	65.260	69.285	73.177	76.969	80.683	84.334	87.933	91.489	95.008
p=43	45.852	52.588	57.642	62.166	66.398	70.441	74.348	78.154	81.880	85.543	89.153	92.719	96.248
p=44	46.874	53.653	58.735	63.282	67.534	71.594	75.517	79.336	83.075	86.750	90.371	93.947	97.485
p=45	47.895	54.717	59.828	64.397	68.669	72.745	76.683	80.517	84.268	87.954	91.586	95.172	98.719
p=46	48.916	55.781	60.919	65.511	69.801	73.895	77.848	81.695	85.459	89.156	92.798	96.394	99.951
p=47	49.937	56.843	62.009	66.623	70.932	75.042	79.010	82.871	86.647	90.356	94.009	97.614	101.180
p=48	50.958	57.905	63.098	67.734	72.062	76.188	80.171	84.045	87.834	91.553	95.217	98.832	102.407
p=49	51.978	58.966	64.186	68.844	73.190	77.333	81.330	85.217	89.018	92.749	96.423	100.048	103.632
p=50	52.998	60.026	65.273	69.952	74.316	78.475	82.487	86.387	90.200	93.943	97.627	101.262	104.855
p=51	54.017	61.086	66.358	71.059	75.441	79.616	83.642	87.556	91.381	95.134	98.828	102.473	106.076
p=52	55.037	62.145	67.443	72.164	76.565	80.756	84.796	88.722	92.559	96.324	100.028	103.683	107.294
p=53	56.056	63.203	68.527	73.269	77.687	81.894	85.948	89.887	93.736	97.511	101.226	104.890	108.510
p=54	57.075	64.260	69.609	74.372	78.808	83.030	87.099	91.051	94.911	98.697	102.422	106.096	109.725
p=55	58.093	65.317	70.691	75.474	79.928	84.165	88.248	92.212	96.084	99.881	103.616	107.299	110.937
p=56	59.112	66.373	71.772	76.575	81.046	85.299	89.395	93.372	97.256	101.064	104.809	108.501	112.148
p=57	60.130	67.428	72.852	77.675	82.163	86.431	90.541	94.531	98.426	102.244	105.999	109.701	113.356
p=58	61.148	68.483	73.931	78.774	83.279	87.562	91.686	95.688	99.594	103.423	107.188	110.899	114.563
p=59	62.166	69.537	75.010	79.872	84.394	88.692	92.829	96.843	100.761	104.601	108.375	112.095	115.768